

Impact of H_0 priors on $f(T)$ late time cosmology

Rebecca Briffa,^{1,2} Celia Escamilla-Rivera,³ Jackson Levi Said,^{1,2} Jurgen Mifsud^{1,2} and and Nathan Lee Pullicino^{1,2}

¹Institute of Space Sciences and Astronomy, University of Malta, Malta, MSD 2080.

²Department of Physics, University of Malta, Malta.

³Instituto de Ciencias Nucleares, Universidad Nacional Autónoma de México, Circuito Exterior C.U., A.P. 70-543, México D.F. 04510, México.

Contributing authors: rebecca.briffa.16@um.edu.mt;
celia.escamilla@nucleares.unam.mx; jackson.said@um.edu.mt;
jurgen.mifsud@um.edu.mt; nathan.pullicino.14@um.edu.mt;

Abstract

We present a detailed analysis of the impact of H_0 priors from recent surveys in the literature on the late time cosmology of five $f(T)$ cosmological models using cosmic chronometers, the Pantheon data set, and baryonic acoustic oscillation data. In this work, we use three recently reported values of H_0 that have contributed to the recent H_0 tension problem. We find that these priors have a strong response in these analyses in terms of all the cosmological parameters. In general, our analyses gives much higher values of H_0 when considered against equivalent analyses without priors while, by and large, giving lower values of the matter density parameter. We close with a cross-analysis of each of our model, data set and prior combination choices.

Keywords: Cosmology, Dark Energy

1 Introduction

The growing pressure from the so-called H_0 tension [1–3] has prompted a reconsideration of novel approaches to formulating a consistent cosmological model. On the other hand, the standard model of cosmology, the Λ CDM cosmological model, rests on overwhelming consistency with observational cosmology [4]. This is only possible with the inclusion of matter beyond the standard model of particle physics in terms of cold dark matter (CDM) which stabilizes galactic structures [5, 6] while on larger scales dark energy, through the cosmological constant (Λ) [7, 8], produces the acceleration observed in this regime [9, 10]. While great efforts have been put into the detection of these exotic forms of matter, they remain elusive to direct observations [11], and continue to be plagued by foundational issues [12].

The prospect of a possible observational disparity in Λ CDM has prompted renewed efforts to determine the current value of the cosmological expansion in order to better assess the degree of inconsistency that the concordance model may be expressing. This parameter characterizes the discrepancy between Λ CDM independent measurements of the Hubble parameter at current times [13, 14] and its Λ CDM-based predicted value from early time observations [4, 15]. While tip of the red giant branch (TRGB, Carnegie-Chicago Hubble Program) point to a lower H_0 tension, the H_0 tension has been growing for some time and may only be resolved either by novel observations such as using gravitational astronomy [16–19], or possibly by considering other gravitational contributions to our cosmological model.

There exist many possible modifications of general relativity (GR) that may be further developed into an observationally viable gravitational base for a concordance model for cosmology [20–22]. These are largely built on correction terms to the Einstein-Hilbert action [23, 24]. Here, gravitational interactions continue to be based on the curvature associated with the Levi-Civita connection, which is the source of curvature in GR [25, 26]. However, there is a growing body of work in which torsion rather than curvature is considered as the form in which gravitation is expressed [27–30], which has produced interesting cosmological models. Teleparallel gravity (TG) incorporates the theories in which the teleparallel connection [27, 31] is used, which expresses this torsion in geometry. The teleparallel connection is curvature-less and satisfies metricity, and so all measures of curvature identically vanish irrespective of the components of the metric. A consequence of this is that the regular Ricci scalar $\overset{\circ}{R}$ (over-circles represent quantities calculated with the Levi-Civita connection) will be zero when calculated with the teleparallel connection, i.e. $R = 0$. By relating both forms of the Ricci scalar, TG produces a torsion scalar T which is dynamically equivalent to GR, called the *Teleparallel equivalent of General Relativity* (TEGR), which differs from the Einstein-Hilbert action by a boundary term B . The division between the torsion scalar and boundary terms means that a much larger range of theories that are second-order in derivatives can be formed giving a weaker form of the generalized Lovelock theory [32–34].

Using the same rationale as in other modified theories of gravity, such as $f(\overset{\circ}{R})$ gravity [20, 23, 24], TEGR can be directly generalized to $f(T)$ gravity [35–40]. $f(T)$ gravity is a second-order gravitational theory that has shown promise at meeting the observational challenges that are becoming all the more pressing [29, 41–45]. In Ref. [46] both expansion and growth data are used to constrain several prominent models of $f(T)$ gravity, resulting in model parameters that are within 1σ of their corresponding Λ CDM values where specific extended models are considered. The three most promising extended models are then reconsidered in Ref. [47] where the most recent observations are considered, and which shows consistency with Λ CDM. $f(T)$ gravity has also been analyzed in terms of its impact on the CMB power spectrum from gravitational waves where in Ref. [48] the power-law model was explored in this regime. More recently, Ref. [49] include data from big bang nucleosynthesis to constrain further these three models.

In recent years there have been a number of cosmology independent measurements of the current value of Hubble parameter, which is the main driver of the growing tension between local, and early-Universe predicted values of H_0 . In this work, we explore the impact of these priors on five core models in $f(T)$ cosmology. The literature contains several additional works where observational data is used to constrain TG models with various uses of priors in these models. To explore the impact of these values of measurements of H_0 we perform several background studies on these models using these various settings in order to better discern the impacts of priors and $f(T)$ models.

TG also produces other interesting theories such as $f(T, B)$ gravity [50–53, 53–58] where the boundary term plays a more active role, as well as $f(T, T_G)$ where T_G is the Gauss-Bonnet invariant [59–62], and numerous scalar-tensor theories such as [34, 63, 64]. We first describe the technical details of TG and its modification to $f(T)$ gravity in Sec. 2, while in Sec. 3 we describe the data sets we use in our Markov chain Monte Carlo (MCMC) implementation. Our core results are presented in Sec. 4 where we also introduce the five models under consideration. We close with a summary of our results and their place against similar studies in the literature in Sec. 5.

2 $f(T)$ FLRW Cosmology

TG recasts the curvature of GR and its modifications [21] with a torsional geometric framework [65] which is built on the exchange of the Levi-Civita connection with the teleparallel connection. This then envelopes into a gravitational theory that embodies torsion from its foundations [27].

The source of curvature in GR is the Levi-Civita connection $\overset{\circ}{\Gamma}{}^\sigma{}_{\mu\nu}$ (over-circles are used throughout to denote quantities determined using the Levi-Civita connection) rather than the metric tensor, which acts as the dynamical variable of the theory but actually only quantifies the amount of geometric deformation. TG characterizes gravitation as torsion through its associated

teleparallel connection $\Gamma^\sigma{}_{\mu\nu}$ which satisfies metricity but which is curvatureless [28, 66]. This realization means that all the curvature-based quantities will identically vanish for the teleparallel connection such as the teleparallel Riemann tensor (the regular Levi-Civita connection Riemann tensor naturally does not vanish). In this background, TG requires an entirely new formulation of gravitational tensors on which to build theories (see reviews in Refs. [28–30]).

The most direct way of formulating teleparallel theories of gravity is through the tetrad $e^A{}_\mu$ (and its inverses $E_A{}^\mu$) which replaces the metric tensor as the fundamental dynamical variable in TG theories through

$$g_{\mu\nu} = e^A{}_\mu e^B{}_\nu \eta_{AB}, \quad \eta_{AB} = E_A{}^\mu E_B{}^\nu g_{\mu\nu}, \quad (1)$$

where Latin indices represent coordinates on the tangent space while Greek indices represent coordinates on the general manifold [29]. In GR, tetrads are largely suppressed in their usage, as an example, they are used to describe spinors [67]. Naturally, tetrads have to satisfy orthogonality conditions

$$e^A{}_\mu E_B{}^\mu = \delta_B^A, \quad e^A{}_\mu E_A{}^\nu = \delta_\mu^\nu, \quad (2)$$

for internal consistency.

The teleparallel connection can be defined as [30, 31]

$$\Gamma^\sigma{}_{\nu\mu} := E_A{}^\sigma (\partial_\mu e^A{}_\nu + \omega^A{}_{B\mu} e^B{}_\nu), \quad (3)$$

where $\omega^A{}_{B\mu}$ is a flat spin connection which is responsible for incorporating the local Lorentz transformation invariance of the theory (which arises explicitly due to the appearance of the tangent space indices). This can be contrasted with GR where the spin connections (associated with their tetrads) are not flat [25]. In TG, tetrad-spin connection pairs represent gravitational and local degrees of freedom respectively and both contribute to a system's equations of motion. Similar to the way that the Levi-Civita connection builds up to the Riemann tensor, the teleparallel connection can be used to describe a torsion tensor [66]

$$T^\sigma{}_{\mu\nu} := 2\Gamma^\sigma{}_{[\nu\mu]}, \quad (4)$$

where square brackets denote an antisymmetric operator, and where $T^\sigma{}_{\mu\nu}$ represents the gauge field strength of gravity in TG [28]. The torsion tensor is covariant under both diffeomorphisms and local Lorentz transformations. By taking suitable contractions of the torsion tensor, a torsion scalar can be written down as [27–30]

$$T := \frac{1}{4} T^\alpha{}_{\mu\nu} T^\alpha{}^{\mu\nu} + \frac{1}{2} T^\alpha{}_{\mu\nu} T^{\nu\mu}{}_\alpha - T^\alpha{}_{\mu\alpha} T^{\beta\mu}{}_\beta, \quad (5)$$

which can be arrived at either by demanding that T be equivalent to the Ricci scalar (up to a boundary term), or by interpreting TG as a gauge theory of translations, which then naturally leads to this form of the torsion scalar. The

Ricci scalar is dependent only on the Levi-Civita connection, and similarly, the torsion scalar is entirely dependent on the teleparallel connection.

Theories based on the Levi-Civita connection produce the Ricci scalar \mathring{R} among other measures of curvature. By exchanging this with the teleparallel connection, this form of the Ricci scalar will identically vanish, meaning $R \equiv 0$ (where we emphasize that $R = R(\Gamma^\sigma_{\mu\nu})$ and $\mathring{R} = \mathring{R}(\mathring{\Gamma}^\sigma_{\mu\nu})$). In terms of gravitational scalars, the torsion and Ricci scalar are equivalent up to a boundary term B , which can be represented through the relation [41, 50]

$$R = \mathring{R} + T - B = 0. \quad (6)$$

This is the base of the TEGR action, which is thus guaranteed to feature identical equations of motion as the Einstein-Hilbert action.

Following the same reasoning as the many extensions to GR, such as $f(\mathring{R})$ gravity [24, 68], TEGR can be arbitrarily extended to $f(T) = -T + \mathcal{F}(T)$ gravity by raising the TEGR action to [35–39, 69]

$$\mathcal{S}_{\mathcal{F}(T)} = \frac{1}{2\kappa^2} \int d^4x e (-T + \mathcal{F}(T)) + \int d^4x e \mathcal{L}_m, \quad (7)$$

where $\kappa^2 = 8\pi G$, \mathcal{L}_m is the matter Lagrangian, and $e = \det(e^a_\mu) = \sqrt{-g}$ is the tetrad determinant. The TEGR limit will then be described by $\mathcal{F}(T) \rightarrow 0$, while Λ CDM is recovered when the arbitrary Lagrangian tends to a constant Λ value. The most important difference, in terms of the dynamical equations, between $\mathcal{F}(\mathring{R})$ and $\mathcal{F}(T)$ is that the total divergence term B (6) is no longer a boundary term in $\mathcal{F}(\mathring{R}) = \mathcal{F}(-T + B)$ gravity. This is the reason why $\mathcal{F}(\mathring{R})$ equations of motion become fourth-order while $f(T)$ remains second-order, as in TEGR. This is advantageous for several reasons such as being naturally Gauss-Ostrogadsky ghost free [28] and being more amenable to numerical approaches.

The field equations for $f(T)$ gravity can then be written as

$$\begin{aligned} W_a{}^\mu := e^{-1} \partial_\nu (e E_a{}^\rho S_\rho{}^{\mu\nu}) (-1 + \mathcal{F}_T) - E_a{}^\lambda T^\rho{}_{\nu\lambda} S_\rho{}^{\nu\mu} (-1 + \mathcal{F}_T) + \frac{1}{4} E_a{}^\mu (-T + \mathcal{F}(T)) \\ + E_a{}^\rho S_\rho{}^{\mu\nu} \partial_\nu (T) \mathcal{F}_{TT} + E_b{}^\lambda \omega^b{}_{a\nu} S_\lambda{}^{\nu\mu} (-1 + \mathcal{F}_T) = \kappa^2 E_a{}^\rho \Theta_\rho{}^\mu, \end{aligned} \quad (8)$$

where subscripts denote derivatives ($\mathcal{F}_T = \partial\mathcal{F}/\partial T$ and $\mathcal{F}_{TT} = \partial^2\mathcal{F}/\partial T^2$), and $\Theta_\rho{}^\nu$ is the regular energy-momentum tensor. The separate tetrad and spin connection variations produce the field equations [27]

$$W_{(\mu\nu)} = \kappa^2 \Theta_{\mu\nu}, \quad \text{and} \quad W_{[\mu\nu]} = 0, \quad (9)$$

which represent the degrees of freedom associated with the tetrad and spin connection, respectively. For any metric ansatz a unique tetrad-spin connection

pair exists such that the local frame is compatible with all the spin connection components vanishing, which is called the Weitzenböck gauge [27, 30]. In this setting, $W_{[\mu\nu]}$ vanishes taking a select choice of tetrad components, while still satisfying the metric equations in Eq. (1).

In this work we explore the cosmology of a flat homogeneous and isotropic Universe which can be represented by the tetrad [70, 71]

$$e^A{}_\mu = \text{diag}(1, a(t), a(t), a(t)) , \quad (10)$$

where $a(t)$ is the scale factor in cosmic time t , and which was shown to universally satisfy the Weitzenböck gauge conditions in Ref. [65]. This reproduces, through Eq. (1), the regular flat Friedmann–Lemaître–Robertson–Walker (FLRW) metric [25]

$$ds^2 = dt^2 - a^2(t) (dx^2 + dy^2 + dz^2) . \quad (11)$$

Taking the standard definition of Hubble parameter as $H = \dot{a}/a$ where over-dots refer to derivatives with respect to cosmic time, the equivalence in Eq. (6). In this setting, we find $T = -6H^2$ and $B = -6(3H^2 + \dot{H})$, which produces the regular Ricci scalar through

$$\mathring{R} = -T + B = -6(2H^2 + \dot{H}) . \quad (12)$$

The Friedmann equations can then be written down as [27]

$$H^2 + \frac{T}{3}\mathcal{F}_T - \frac{\mathcal{F}}{6} = \frac{\kappa^2}{3}\rho , \quad (13)$$

$$\dot{H}(1 - \mathcal{F}_T - 2T\mathcal{F}_{TT}) = -\frac{\kappa^2}{2}(\rho + p) , \quad (14)$$

where we denote the energy density and pressure of the total matter sector by ρ and p , respectively.

3 Observational Data

We here present the observational data sets which will be considered in the below analyses. For our baseline data set, we consider $H(z)$ data along with a Supernovae type Ia (SNIa) compilation data set.

- For the Hubble parameter data, we adopt thirty-one data points which were inferred via the cosmic chronometers (CC) technique. Such a technique enables us to directly derive information about the Hubble function at several redshifts, up to $z \lesssim 2$. Since the adopted CC data is primarily based on measurements of the age difference between two passively-evolving galaxies that formed at the same time but are separated by a small redshift interval

(from which one can compute $\Delta z/\Delta t$), CC were found to be more reliable than any other method based on an absolute age determination for galaxies [72]. Our adopted CC data points were compiled from Refs. [73–79], which are independent of the Cepheid distance scale and from any cosmological model, although they are dependent on the modelling of stellar ages, which is based on robust stellar population synthesis techniques (see, for instance, Refs. [75, 77, 80–83] for analyses related to CC systematics). The corresponding χ_H^2 estimator is given by

$$\chi_H^2(\Theta) = \sum_{i=1}^{31} \frac{(H(z_i, \Theta) - H_{\text{obs}}(z_i))^2}{\sigma_H^2(z_i)}, \quad (15)$$

where $H(z_i, \Theta)$ are the theoretical Hubble parameter values at redshift z_i with model parameters Θ , $H_{\text{obs}}(z_i)$ are the corresponding measured values of the Hubble parameter at z_i with observational error of $\sigma_H(z_i)$.

- The other component of our baseline data set consists of the Pantheon compilation of 1048 SNIa relative luminosity distance measurements spanning the redshift range of $0.01 < z < 2.3$ [84]. Henceforth, we will be denoting the Pantheon SNIa compilation by SN. The publicly available release of the SN catalog provides SNIa magnitudes corrected for systematic effects, including the stretch of the light–curve, the color at maximum brightness and the stellar mass of the host galaxy. Since the apparent magnitude of each SNIa needs to be calibrated via an arbitrary fiducial absolute magnitude M , we will be considering M as a nuisance parameter in our MCMC analyses. This can be implemented through the use of the theoretical values of the distance moduli

$$\mu(z_i, \Theta) = 5 \log_{10} [D_L(z_i, \Theta)] + M, \quad (16)$$

at redshift z_i via the corresponding computation of the luminosity distance

$$D_L(z_i, \Theta) = c (1 + z_i) \int_0^{z_i} \frac{dz'}{H(z', \Theta)}, \quad (17)$$

where c is the speed of light, and the nuisance parameter M encodes the Hubble constant which has to be marginalized over in the MCMC analyses. The associated χ_{SN}^2 is specified by [85]

$$\chi_{\text{SN}}^2(\Theta) = (\Delta\mu(z_i, \Theta))^T C_{\text{SN}}^{-1} \Delta\mu(z_i, \Theta) + \ln \left(\frac{S}{2\pi} \right) - \frac{k^2(\Theta)}{S}, \quad (18)$$

where C_{SN} is the total covariance matrix, S is the sum of all the components of C_{SN}^{-1} , while k is given by

$$k(\Theta) = (\Delta\mu(z_i, \Theta))^T \cdot C_{\text{SN}}^{-1}, \quad (19)$$

with $\Delta\mu(z_i, \Theta) = \mu(z_i, \Theta) - \mu_{\text{obs}}(z_i)$.

- We further consider a joint baryon acoustic oscillation (BAO) data set composed of independent data points. The BAO data set incorporates the SDSS Main Galaxy Sample measurement at $z_{\text{eff}} = 0.15$ [86], the six-degree Field Galaxy Survey measurement at $z_{\text{eff}} = 0.106$ [87], and the BOSS DR11 quasar Lyman- α measurement at $z_{\text{eff}} = 2.4$ [88]. We further consider the angular diameter distances and $H(z)$ measurements of SDSS-IV eBOSS DR14 quasar survey at $z_{\text{eff}} = \{0.98, 1.23, 1.52, 1.94\}$ [89], along with the SDSS-III BOSS DR12 consensus BAO measurements of the Hubble parameter and the corresponding comoving angular diameter distances at $z_{\text{eff}} = \{0.38, 0.51, 0.61\}$ [90], where in these two BAO data sets we consider the full covariance matrix in our MCMC analyses. For the considered BAO data sets we computed the Hubble distance $D_H(z)$, comoving angular diameter distance $D_M(z)$, and volume-average distance $D_V(z)$, which are respectively specified by

$$D_H(z) = \frac{c}{H(z)}, \quad D_M(z) = (1+z)D_A(z), \quad D_V(z) = \left[(1+z)^2 D_A^2(z) \frac{z}{H(z)} \right]^{1/3}, \quad (20)$$

with $D_A(z) = (1+z)^{-2}D_L(z)$ being the angular diameter distance. In order to use the reported BAO results in our MCMC analyses, we had to consider the corresponding combination of parameters $\mathcal{G}(z_i) = \{D_V(z_i)/r_s(z_d), r_s(z_d)/D_V(z_i), D_H(z_i), D_M(z_i)(r_{s,\text{fid}}(z_d)/r_s(z_d)), H(z_i)(r_s(z_d)/r_{s,\text{fid}}(z_d)), D_A(z_i)(r_{s,\text{fid}}(z_d)/r_s(z_d))\}$, for which we had to compute the comoving sound horizon $r_s(z)$ at the end of the baryon drag epoch at redshift $z_d \approx 1059.94$ [4], such that

$$r_s(z) = \int_z^\infty \frac{c_s(\tilde{z})}{H(\tilde{z})} dz = \frac{1}{\sqrt{3}} \int_0^{1/(1+z)} \frac{da}{a^2 H(a) \sqrt{1 + [3\Omega_{b,0}/(4\Omega_{\gamma,0})] a}}, \quad (21)$$

where we have adopted $\Omega_{b,0} = 0.02242$ [4], $T_0 = 2.7255$ K [91], and a fiducial value of $r_{s,\text{fid}}(z_d) = 147.78$ Mpc. The corresponding $\chi_{\text{BAO}}^2(\Theta)$ is specified by

$$\chi_{\text{BAO}}^2(\Theta) = (\Delta\mathcal{G}(z_i, \Theta))^T C_{\text{BAO}}^{-1} \Delta\mathcal{G}(z_i, \Theta), \quad (22)$$

where $\Delta\mathcal{G}(z_i, \Theta) = \mathcal{G}(z_i, \Theta) - \mathcal{G}_{\text{obs}}(z_i)$, and C_{BAO} is the covariance matrix of all the considered BAO observations.

Further to the above data sets, we will also be analysing the impact of an H_0 prior value on our $f(T)$ model parameter constraints. We will be considering the latest SH0ES local estimate [13] of $H_0 = 74.22 \pm 1.82$ km s $^{-1}$ Mpc $^{-1}$ (R19) based on SN in the Hubble flow, the H0LiCOW Collaboration's [14] measurement which relies on strong lensing from quasars and has a value of $73.3_{-1.8}^{+1.7}$ km s $^{-1}$ Mpc $^{-1}$ (HW), and finally the measurement using the tip of the red giant branch (TRGB) as a standard candle with $H_0 = 69.8 \pm 1.9$ km s $^{-1}$ Mpc $^{-1}$ [92]. While other measurements exist (see, for instance, Ref. [17]), the aforementioned measurements are the most representative

model-independent local values which have been exhaustively studied in the literature.

4 Constraints of $f(T)$ Cosmological Models

We take five models within the $f(T)$ gravity framework in which to probe the impact of recent cosmology model independent measurements of H_0 . These have gained prominence in the literature and are frequently studied since they are reported to mirror very well our cosmological history. We analyze the impact that these priors have on the resulting parameter values for the data sets described in Sec. 3. In this context, we try to separate the impacts between the choice of prior on H_0 and the $f(T)$ model under consideration.

In order to better evaluate the performance of each f_i CDM model against Λ CDM, we compute the Akaike information criterion (AIC) [93] to assess which model ultimately best supports the data. The AIC is defined as

$$\text{AIC} = -2 \ln L_{\max} + 2n, \quad (23)$$

where L_{\max} is the maximum value of the likelihood function for each model and data set together with prior combination, and n is the number of parameters involved in the estimation routine. In practice, lower values of AIC indicate better performance against observational data set combinations. On the other hand, we also consider the Bayesian information criterion (BIC) [94] which is closely related to AIC and defined as

$$\text{BIC} = -2 \ln L_{\max} + n \ln m, \quad (24)$$

where m is the sample size of the observational data combination. This variant of the AIC also imposes a penalty for models having a large number of parameters to estimate, which is more impactful in BIC. The explicit appearance of the number of points in a data set also makes the BIC an arguably better measure of the performance of AIC against observational data.

4.1 $f_1(T)$ CDM Model

The power-law model [37] was first explored due to its ability to produce an accelerated late-time Universe. This model is expressed as

$$\mathcal{F}_1(T) = \alpha_1 (-T)^{b_1}, \quad (25)$$

where α_1 and b_1 are constants. By evaluating the Friedmann equation (13) at current times, we can obtain

$$\alpha_1 = (6H_0^2)^{1-b_1} \frac{1 - \Omega_{M_0}}{1 - 2b_1}, \quad (26)$$

where $\Omega_{M_0} = \Omega_{m_0} + \Omega_{r_0}$, and where Ω_{m_0} and Ω_{r_0} are the density parameters for matter and radiation at current times, respectively. This makes b_1 the only new model parameter for f_1 CDM rather than the superficial addition of two parameters shown in Eq. (25).

By defining the normalised Hubble parameter $E(z) := H(z)/H_0$, we can write the Friedmann equation 13 for this model as

$$E^2(z) = \Omega_{m_0} (1+z)^3 + \Omega_{r_0} (1+z)^4 + (1 - \Omega_{m_0} - \Omega_{r_0}) E^{2b_1}(z), \quad (27)$$

which reduces to the Λ CDM model for $b_1 = 0$, and to the Dvali, Gabadadze and Porrati (DGP) [95, 96] model for $b_1 = 1/2$. For $b_1 = 1$, the additional component in the Friedmann equation produces a rescaled gravitational constant term in the density parameters, i.e. this is the pure GR limit. This gives an upper bound such that $b_1 < 1$ for an accelerating Universe.

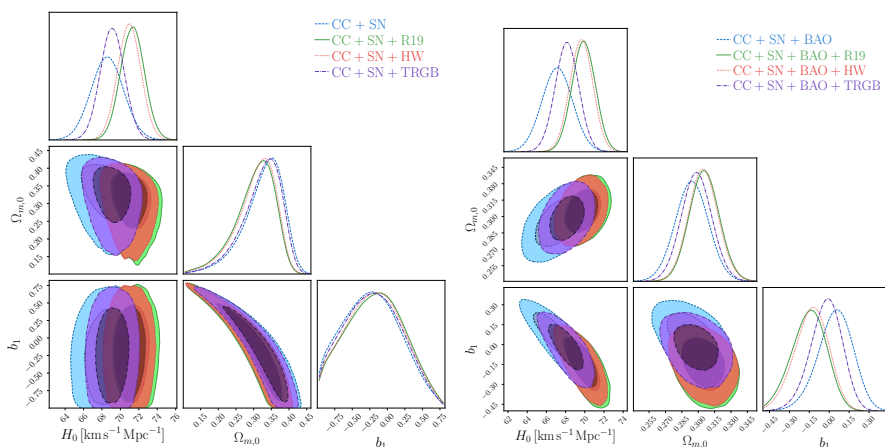


Fig. 1 *Left*: Confidence levels (C.L.) and posteriors for the f_1 CDM (Power Law) model (25) using CC+SN data along the H_0 priors: R19 (green color), HW (red color) and TRGB (purple color), are respectively shown. *Right*: C.L. and posteriors for the Power Law model (25) using CC+SN+BAO data are shown using the same prior colors.

In Fig. 1, the posteriors and confidence regions are shown for both CC+SN and CC+SN+BAO data set combinations. In these plots, we also show the results for each of the priors on H_0 which are described in Sec. 3. Immediately, one notices that the biggest impact of having a prior is to raise the value of H_0 in the results from the scenario in which there is no prior. A similar effect occurs for the $\Omega_{m,0}$ parameter but this is less pronounced.

To see the precision values, we give specific results in Table 1 where it becomes clear that the highest value of the Hubble constant is achieved for the CC+SN data set with an R19 prior ($H_0 = 71.3^{+1.3}_{-1.4} \text{kms}^{-1} \text{Mpc}^{-1}$) which occurs due to early Universe impacts on BAO data having the effect of reducing the value of the H_0 parameter while R19 being the highest prior produces a shift

Table 1 Results for the f_1 CDM (Power Law) model (25). First column: data sets used to constrain the model, including the H_0 priors. Second column: H_0 values derived from the analysis. Third column: Constrained $\Omega_{m,0}$. Fourth column: Best fit b_1 values. Fifth column: Nuisance parameter, M . Sixth column: χ^2_{\min} . From seventh up to tenth column: AIC and BIC with their respective differences with Λ CDM within the corresponding data set and prior combination (as shown in Appendix A).

Data Sets	H_0 [km/s/Mpc]	$\Omega_{m,0}$	b_1	M	χ^2_{\min}	AIC	BIC	Δ AIC	Δ BIC
CC + SN	68.5 ± 1.8	$0.350^{+0.045}_{-0.064}$	$-0.22^{+0.41}_{-0.48}$	$-19.390^{+0.053}_{-0.055}$	1040.94	1048.94	1068.88	1.45	6.43
CC + SN + R19	$71.3^{+1.3}_{-1.4}$	$0.326^{+0.045}_{-0.065}$	$-0.13^{+0.40}_{-0.50}$	$-19.314^{+0.039}_{-0.038}$	1045.83	1053.83	1073.77	1.51	6.50
CC + SN + HW	71.0 ± 1.3	$0.329^{+0.045}_{-0.062}$	$-0.16^{+0.41}_{-0.48}$	$-19.324^{+0.038}_{-0.037}$	1044.50	1052.50	1072.44	1.51	6.50
CC + SN + TRGB	$69.1^{+1.4}_{-1.3}$	$0.344^{+0.045}_{-0.063}$	$-0.20^{+0.42}_{-0.47}$	-19.375 ± 0.040	1041.55	1049.55	1069.49	1.87	6.85
CC + SN + BAO	67.1 ± 1.6	0.294 ± 0.015	0.06 ± 0.13	-19.435 ± 0.047	1057.13	1065.13	1085.13	1.68	6.68
CC + SN + BAO + R19	69.9 ± 1.2	$0.305^{+0.014}_{-0.013}$	$-0.14^{+0.12}_{-0.13}$	$-19.359^{+0.035}_{-0.034}$	1066.87	1074.87	1094.87	0.56	5.56
CC + SN + BAO + HW	69.7 ± 1.2	$0.304^{+0.014}_{-0.012}$	$-0.12^{+0.12}_{-0.13}$	$-19.366^{+0.035}_{-0.033}$	1064.92	1072.92	1086.92	0.89	5.89
CC + SN + BAO + TRGB	68.1 ± 1.2	0.298 ± 0.014	$-0.01^{+0.11}_{-0.12}$	-19.407 ± 0.036	1058.56	1066.56	1086.56	2.00	7.00

to higher values in the MCMC runs. In tandem, the value of $\Omega_{m,0}$ reaches a minimum for the CC+SN data set for the R19 prior, which tallies with having a large value of H_0 since most of the energy in this scenario will appear as an effective dark energy. Following a similar reasoning, the lowest value of the Hubble constant appears for the no prior ($H_0 = 67.1 \pm 1.6 \text{ km s}^{-1} \text{ Mpc}^{-1}$) scenario in which CC+SN+BAO data set is selected. Here, the combination of BAO data and the impact of not assuming a prior on H_0 brings the value of the Hubble constant to its lowest point. Conversely, this raises the value of $\Omega_{m,0}$ to its highest value for the CC+SN+BAO data set.

In all cases, the value of the b_1 parameter is found to be within 1σ of their corresponding Λ CDM value except for the CC+SN+BAO with an R19 prior run where this moves to being within 2σ of the corresponding Λ CDM value. Coincidentally, from the array of all the MCMC runs, this run also turns out to give the lowest values of both Δ AIC and Δ BIC in comparison to the respective Λ CDM run which is interesting since this becomes the favoured model of the group of runs. On the other hand, the b_4 parameter may effect cosmic perturbations giving an intriguing division between background and perturbation behaviour in terms of model parameters.

These results are within the confidence regions of previous studies in the literature [46, 49, 97, 98] for the closest prior value. We nuance these results in the literature with more in-depth analysis of the impact of other priors on the eventual cosmological parameter values.

4.2 $f_2(T)$ CDM Model

The Linder model [38] was designed to produce late-time accelerated expansion and is described by

$$\mathcal{F}_2(T) = \alpha_2 T_0 \left(1 - \text{Exp} \left[-b_2 \sqrt{T/T_0} \right] \right), \quad (28)$$

where α_2 and b_2 are constants, and where $T_0 = T|_{t=t_0} = 6H_0^2$. Evaluating at current times, the Friedmann equation relates these constants through

$$\alpha_2 = \frac{1 - \Omega_{M_0}}{(1 + b_2) e^{-b_2} - 1}, \quad (29)$$

which makes b_2 the new parameter for the f_2 CDM model. The corresponding Friedmann equation can then be written as

$$E^2(z) = \Omega_{m_0} (1+z)^3 + \Omega_{r_0} (1+z)^4 + \frac{1 - \Omega_{m_0} - \Omega_{r_0}}{(b_2 + 1) e^{-b_2} - 1} [(1 + b_2 E(z)) \text{Exp}[-b_2 E(z)] - 1], \quad (30)$$

which reduces to Λ CDM as $b_2 \rightarrow +\infty$. We perform our analysis for $1/b_2$ so that this limit becomes $1/b_2 \rightarrow 0^+$, which also makes the numerical approach more stable.

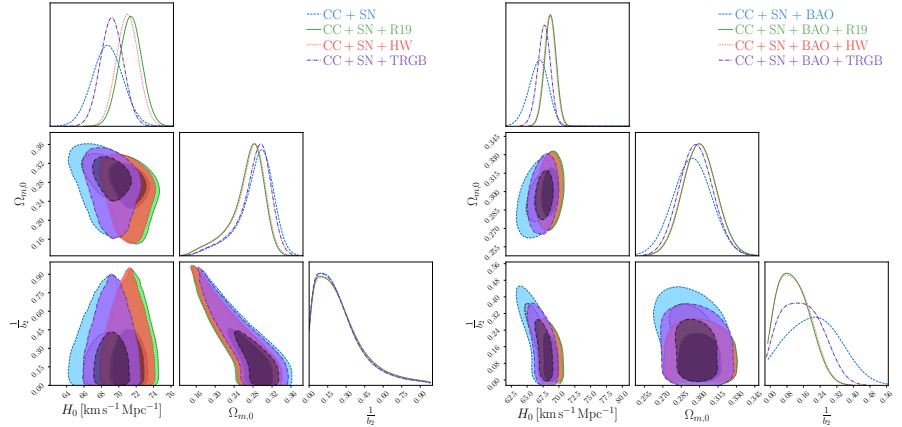


Fig. 2 *Left*: C.L and posteriors for the f_2 CDM (Linder) model (28) using CC+SN data along the H_0 priors: R19 (green color), HW (red color) and TRGB (purple color), respectively. *Right*: C.L and posteriors for the Linder model (28) using CC+SN+BAO data along the same priors denoted.

For this case, we show the posteriors and confidence regions of all the output MCMC runs in Fig. 2. Some similar patterns to the f_1 CDM model emerge such as priors on H_0 pushing the value of the Hubble constant from the MCMC runs to higher values, and some anti-correlation between $\Omega_{m,0}$ and the model parameter b_i . However, this is a different model and has different properties. By design, this naturally leads to an accelerating late time Universe [38], which we do confirm in this case and, in fact we get slightly higher values for the expansion rate when compared with the f_1 CDM power-law model.

In Table. 2, we show the precision outputs for each of the MCMC runs together with their settings for priors on H_0 . While slightly higher, we again find that the largest H_0 is achieved for the CC+SN data set with an R19 prior

Table 2 Results for the f_2 CDM (Linder) model (28). First column: data sets used to constrain the model, including the H_0 priors. Second column: H_0 values derived from the analysis. Third column: Constrained $\Omega_{m,0}$. Fourth column: Best fit $1/b_2$ values. Fifth column: Nuisance parameters, M . Sixth column: χ^2_{\min} . From seventh up to tenth column: AIC and BIC with their respective differences with Λ CDM within the corresponding data set and prior combination (as shown in Appendix A).

Data Sets	H_0 [km/s/Mpc]	$\Omega_{m,0}$	$\frac{1}{b_2}$	M	χ^2_{\min}	AIC	BIC	Δ AIC	Δ BIC
CC + SN	$68.7^{+1.8}_{-1.7}$	$0.298^{+0.031}_{-0.035}$	$0.101^{+0.227}_{-0.098}$	$-19.43^{+0.57}_{-0.47}$	1041.49	1049.49	1069.43	2.00	6.98
CC + SN + R19	71.4 ± 1.3	$0.283^{+0.027}_{-0.036}$	$0.088^{+0.252}_{-0.086}$	$-19.28^{+0.50}_{-0.51}$	1046.32	1054.32	1074.25	2.00	6.99
CC + SN + HW	$71.0^{+1.3}_{-1.2}$	$0.285^{+0.027}_{-0.036}$	$0.096^{+0.245}_{-0.093}$	$-19.37^{+0.45}_{-0.34}$	1044.99	1052.99	1072.93	2.00	6.99
CC + SN + TRGB	69.2 ± 1.3	$0.296^{+0.028}_{-0.035}$	$0.088^{+0.239}_{-0.085}$	$-19.36^{+0.36}_{-0.37}$	1041.69	1049.69	1069.62	2.00	6.99
CC + SN + BAO	$66.9^{+1.5}_{-1.6}$	0.294 ± 0.016	$0.22^{+0.12}_{-0.15}$	$-19.38^{+0.22}_{-0.35}$	1056.52	1064.62	1084.52	1.06	6.06
CC + SN + BAO + R19	$68.71^{+0.88}_{-0.96}$	0.300 ± 0.014	$0.079^{+0.098}_{-0.064}$	$-19.35^{+0.19}_{-0.24}$	1068.31	1076.31	1096.31	2.00	7.00
CC + SN + BAO + HW	$68.58^{+0.89}_{-0.92}$	$0.300^{+0.013}_{-0.014}$	$0.076^{+0.105}_{-0.060}$	$-19.389^{+0.045}_{-0.047}$	1066.03	1074.03	1094.03	2.00	7.00
CC + SN + BAO + TRGB	67.7 ± 1.0	0.297 ± 0.014	$0.128^{+0.111}_{-0.099}$	$-19.46^{+0.37}_{-0.26}$	1058.47	1066.47	1086.47	1.90	6.90

($H_0 = 71.4 \pm 1.3 \text{ km s}^{-1} \text{ Mpc}^{-1}$) which is an expected feature as in f_1 CDM. In tandem, we then find the lowest value of $\Omega_{m,0}$ for this MCMC run in this data set. Analogously, the CC+SN+BAO MCMC run with no prior ($H_0 = 66.9^{+1.5}_{-1.6} \text{ km s}^{-1} \text{ Mpc}^{-1}$) gives the least expanding cosmology. Given how close the R19 and HW priors are in value, in all the MCMC runs, they always gave comparatively similar results for the ensuing cosmological parameters.

For numerical stability we take $1/b_2$ to be the active parameter in our MCMC runs, which means that the Λ CDM limit would be represented by $1/b_2 \rightarrow 0^+$. Dissimilar to f_1 CDM, most models fall within a 2σ rather than 1σ making them slightly further away from favouring Λ CDM directly. Another curious feature of the results is that despite each of the Δ AIC and Δ BIC being calculated for each corresponding data set and prior combination for Λ CDM, it turns out that most Δ AIC and Δ BIC values tend to about 2.0 and 6.99 respectively, with the closest to Λ CDM being the CC+SN+BAO with no prior setting. Given that BAO depends on the early Universe to some extent, this is not an unexpected result for the model.

While still consistent with the literature in Refs. [46, 49, 97, 98], the various priors do add a lot more detail to the impact of the priors on H_0 and their effect on the MCMC runs and the resulting model parameter values. For instance, the priors by and large reduce the uncertainties in the resulting parameters which is interesting for purposes of comparison with Λ CDM.

4.3 $f_3(T)$ CDM Model

Motivated by works in $f(\dot{R})$ gravity [99], Ref. [46] proposes the following variant of the Linder model

$$\mathcal{F}_3(T) = \alpha_3 T_0 (1 - \text{Exp}[-b_3 T/T_0]) , \quad (31)$$

where α_3 and b_3 are constants, which can be related through

$$\alpha_3 = \frac{1 - \Omega_{M_0}}{(1 + 2b_3)e^{-b_3} - 1}, \quad (32)$$

where the Friedmann equation (13) was evaluated at current times. Thus, the Friedmann equation can be written as

$$E^2(z) = \Omega_{m_0}(1+z)^3 + \Omega_{r_0}(1+z)^4 + \frac{1 - \Omega_{m_0} - \Omega_{r_0}}{(1 + 2b_3)e^{-b_3} - 1} [(1 + 2b_3E^2(z)) \text{Exp}[-b_3E^2(z)] - 1] \quad (33)$$

which tends to Λ CDM as $b_3 \rightarrow +\infty$ similar to f_2 CDM. As in f_2 CDM, we again perform our analysis for $1/b_3$ so that the analysis is more stable. In this case, the Λ CDM limits comes as $1/b_3 \rightarrow 0^+$.

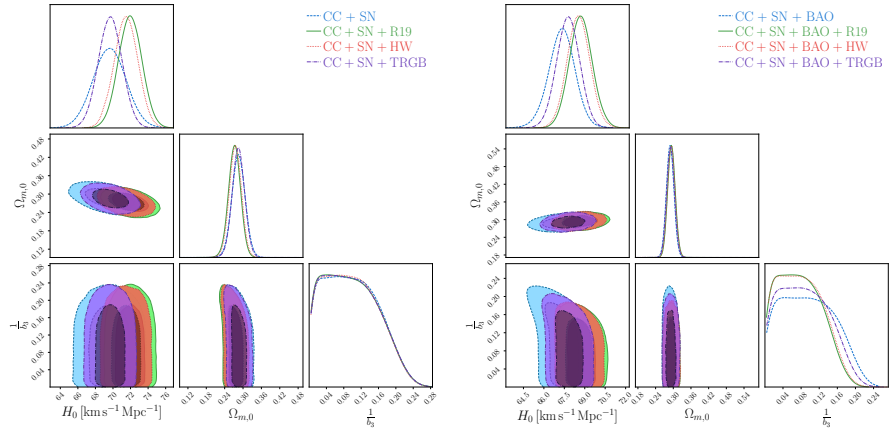


Fig. 3 *Left:* C.L and posteriors for the f_3 CDM model (31) using CC+SN data along the H_0 priors: R19 (green color), HW (red color) and TRGB (purple color), respectively. *Right:* C.L and posteriors for the model (31) using CC+SN+BAO data along the same priors denoted.

The posterior and confidence regions for the f_3 CDM model are shown in Fig. 3. This is an interesting model since in removing the square root in the exponential index there is a clear impact on the confidence regions on $\Omega_{m,0}$ which now has tighter confidence regions, while H_0 is largely left unaffected. Saying that, we again see margin increases in the value of H_0 for some data set and prior settings.

The precision values shown in Table. 3 make clearer the stricter confidence levels in the density parameter values which certainly helps understand the predictions of the model better. As in the previous models, we again see the impact of priors producing a shift of the value of H_0 to higher values, as would be expected. Also, we observe a mildly higher maximum value

Table 3 Results for the f_3 CDM model (31). First column: data sets used to constrain the model, including the H_0 priors. Second column: H_0 values derived from the analysis. Third column: Constrained $\Omega_{m,0}$. Fourth column: Best fit $1/b_3$ values. Fifth column: Nuisance parameter, M . Sixth column: χ^2_{\min} . From seventh up to tenth column: AIC and BIC with their respective differences with Λ CDM within the corresponding data set and prior combination (as shown in Appendix A).

Data Sets	H_0 [km/s/Mpc]	$\Omega_{m,0}$	$\frac{1}{b_3}$	M	χ^2_{\min}	AIC	BIC	Δ AIC	Δ BIC
CC + SN	$69.6^{+1.8}_{-1.9}$	$0.286^{+0.021}_{-0.023}$	$0.067^{+0.078}_{-0.054}$	$-19.367^{+0.053}_{-0.056}$	1045.04	1053.04	1072.97	5.55	10.53
CC + SN + R19	$72.0^{+1.3}_{-1.4}$	0.273 ± 0.020	$0.042^{+0.099}_{-0.032}$	$-19.302^{+0.037}_{-0.039}$	1048.16	1056.16	1076.10	3.84	8.82
CC + SN + HW	71.5 ± 1.4	$0.275^{+0.019}_{-0.020}$	$0.070^{+0.072}_{-0.058}$	$-19.317^{+0.039}_{-0.038}$	1047.06	1055.07	1075.01	4.08	9.06
CC + SN + TRGB	$69.7^{+1.3}_{-1.4}$	$0.285^{+0.020}_{-0.021}$	$0.048^{+0.094}_{-0.037}$	-19.366 ± 0.040	1045.04	1053.04	1072.98	5.36	10.34
CC + SN + BAO	$67.35^{+0.94}_{-0.97}$	0.289 ± 0.013	$0.043^{+0.101}_{-0.026}$	$-19.441^{+0.032}_{-0.031}$	1060.55	1068.55	1088.55	5.09	10.09
CC + SN + BAO + R19	$68.70^{+0.84}_{-0.85}$	$0.293^{+0.013}_{-0.012}$	$0.059^{+0.056}_{-0.047}$	$-19.397^{+0.029}_{-0.028}$	1071.71	1079.71	1099.71	5.41	10.41
CC + SN + BAO + HW	$68.52^{+0.85}_{-0.82}$	$0.295^{+0.011}_{-0.014}$	$0.034^{+0.089}_{-0.024}$	$-19.401^{+0.028}_{-0.029}$	1069.03	1077.03	1097.03	4.99	9.10
CC + SN + BAO + TRGB	67.79 ± 0.85	$0.292^{+0.012}_{-0.014}$	$0.074^{+0.057}_{-0.059}$	$-19.425^{+0.027}_{-0.030}$	1061.78	1069.78	1089.78	5.21	10.21

of the Hubble constant ($H_0 = 72.0^{+1.3}_{-1.4} \text{kms}^{-1} \text{Mpc}^{-1}$) with almost Gaussian errors, while the lowest value is also slightly increased with this model ($H_0 = 67.35^{+0.94}_{-0.97} \text{kms}^{-1} \text{Mpc}^{-1}$).

Now, along the same lines of reasoning as in the f_2 CDM model, we take $1/b_3$ as our parameter in the MCMC runs for the numerical stability of this model. While the mean values are closer to their Λ CDM limits, the confidence regions still point to a largely 2σ distance between the f_3 CDM and Λ CDM models. On the other hand, the Δ AIC and Δ BIC classifiers now give a range of values for the different MCMC settings. However, in this case, the runs favour the CC+SN MCMC run with an R19 prior.

The results presented in Fig. 3 and Table. 3 are consistent with those reported in Refs. [46, 49, 97, 98]. However, the addition of other priors shows how the value of H_0 can also be smaller.

4.4 $f_4(T)$ CDM Model

The logarithmic model, proposed in Ref. [100], is described by

$$\mathcal{F}_4(T) = \alpha_4 T_0 \sqrt{\frac{T}{b_4 T_0}} \log \left[\frac{b_4 T_0}{T} \right], \quad (34)$$

where α_4 and b_4 are constants. Evaluating the Friedmann equation at current times gives

$$\alpha_4 = -\frac{(1 - \Omega_{M_0}) \sqrt{b_4}}{2}, \quad (35)$$

which reduces the Friedmann equation (13) to the relatively simple form

$$E^2(z) = \Omega_{m_0} (1+z)^3 + \Omega_{r_0} (1+z)^4 + (1 - \Omega_{m_0} - \Omega_{r_0}) E(z), \quad (36)$$

which interestingly does not feature b_4 , meaning that background data cannot constrain this parameter. Another important point to highlight is that no

choice of parameter values can reproduce Λ CDM for f_4 CDM. On the other hand, the background behavior of this model does coincide with that of a spatially at self-accelerating branch of the DGP braneworld model [95, 101]. Models of this kind are intriguing because they cannot feature confirmation bias with Λ CDM.

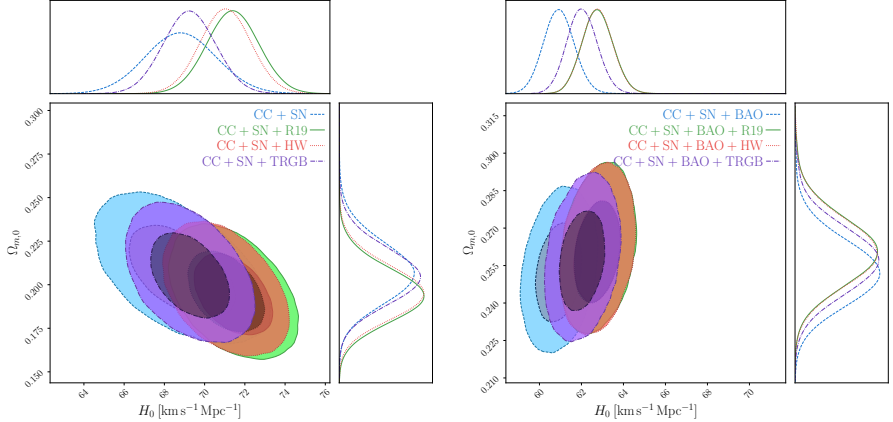


Fig. 4 *Left*: C.L and posteriors for the f_4 CDM model (34) using CC+SN data along the H_0 priors: R19 (green color), HW (red color) and TRGB (purple color), respectively. *Right*: C.L and posteriors for the model (34) using CC+SN+BAO data along the same priors denoted.

Table 4 Results for the Logarithmic model (34). First column: data sets used to constrain the model, including the H_0 priors. Second column: H_0 values derived from the analysis. Third column: Constrained $\Omega_{m,0}$. Fourth column: Nuisance parameter, M . Fifth column: χ^2_{\min} . From sixth up to ninth column: AIC and BIC with their respective differences with Λ CDM within the corresponding data set and prior combination (as shown in Appendix A).

Data Sets	H_0 [km/s/Mpc]	$\Omega_{m,0}$	M	χ^2_{\min}	AIC	BIC	Δ AIC	Δ BIC
CC+ SN	$68.8^{+1.8}_{-1.7}$	$0.207^{+0.018}_{-0.017}$	$-19.371^{+0.051}_{-0.052}$	1043.46	1042.46	1064.41	1.97	1.97
CC + SN + R19	71.4 ± 1.3	$0.194^{+0.016}_{-0.015}$	$-19.301^{+0.038}_{-0.035}$	1047.98	1053.98	1068.94	1.67	1.67
CC + SN + HW	$71.0^{+1.3}_{-1.2}$	$0.195^{+0.016}_{-0.015}$	-19.309 ± 0.036	1046.70	1052.70	1067.65	1.70	1.70
CC + SN + TRGB	69.2 ± 1.3	0.205 ± 0.016	$-19.358^{+0.037}_{-0.040}$	1043.60	1049.60	1064.55	1.91	1.91
CC + SN + BAO	$60.89^{+0.75}_{-0.71}$	$0.252^{+0.014}_{-0.013}$	$-19.611^{+0.027}_{-0.031}$	1078.52	1084.52	1099.52	21.07	21.07
CC + SN + BAO + R19	$62.77^{+0.72}_{-0.76}$	$0.261^{+0.013}_{-0.014}$	$-19.543^{+0.028}_{-0.029}$	1124.87	1130.87	1145.87	56.56	56.56
CC + SN + BAO + HW	$62.77^{+0.70}_{-0.76}$	$0.260^{+0.014}_{-0.013}$	$-19.544^{+0.029}_{-0.028}$	1121.49	1127.49	1142.49	55.47	55.46
CC + SN + BAO + TRGB	$62.02^{+0.72}_{-0.73}$	$0.257^{+0.013}_{-0.014}$	$-19.567^{+0.026}_{-0.033}$	1097.80	1103.80	1118.80	39.23	39.23

For this model, the posteriors and confidence regions are shown in Fig. 4. This is quite an interesting model since it has no Λ CDM limit and so there is no *a priori* expected values for the extra model parameter. Another crucial aspect of the f_4 CDM model is that at background it does not contain any additional parameters in comparison to Λ CDM.

In Table. 4, the precision results are presented for each of the data set and prior combinations. Here a significant difference appears depending on whether BAO data is included or not. For the cases of simply taking CC+SN data, we find reasonable values of H_0 with very low values of $\Omega_{m,0}$ giving a maximum Hubble constant for the R19 prior ($71.4 \pm 1.3 \text{kms}^{-1} \text{Mpc}^{-1}$), as expected. On the other hand, when the BAO data set is included both the Hubble constant and density parameter readings turn out to be very low with a minimum $H_0 = 60.89_{-0.71}^{+0.75} \text{kms}^{-1} \text{Mpc}^{-1}$. In all cases, the uncertainties are tightly constrained due to the small number of parameters.

Nothing can be said about the b_4 parameter from these MCMC runs since the parameter does not appear in the background equations for a flat FLRW cosmology. On the other hand, the statistical indicators tell a different story. For the CC+SN data set, irrespective of whether a prior is put on H_0 or not, the ΔAIC and ΔBIC both turn out to be low in comparison with the respective ΛCDM data set and prior combinations. However, once BAO data is, its not simply the cosmological parameters that start to veer away from their higher confidence observational regions, but also the statistical indicators. Indeed the ΔAIC and ΔBIC in comparison with ΛCDM both become extremely large in this scenario bringing the model into question.

In line with previous studies, [46, 97] we find that logarithmic models do not fair well with observational data, but the addition of BAO data totally removes any possibility of the $f_4\text{CDM}$ model having any significance against observational data.

4.5 $f_5(T)\text{CDM}$ Model

Our last model under consideration is the hyperbolic tangent model given by [102]

$$\mathcal{F}_5(T) = \alpha_5(-T)^{b_5} \text{Tanh}\left(\frac{T_0}{T}\right), \quad (37)$$

where α_5 and b_5 are constants. Using Eq. (13) at current times results in the relation

$$\alpha_5 = \frac{(6H_0^2)^{1-b_5} (1 - \Omega_{M_0})}{(1 - 2b_5)\text{tanh}(1) + 2\text{Sech}^2(1)}. \quad (38)$$

The Friedmann equation can then be written as

$$E^2(z) = \Omega_{m_0} (1+z)^3 + \Omega_{r_0} (1+z)^4 + \frac{1 - \Omega_{m_0} - \Omega_{r_0}}{(2b_5 - 1)\text{tanh}(1) - 2\text{Sech}^2(1)} E^{2(b_5-1)}(z) [(2b_5 - 1)E^2(z)\text{Tanh}(E^{-2}(z)) - 2\text{Sech}^2(E^{-2}(z))]. \quad (39)$$

As in the $f_4\text{CDM}$ model, we do not recover ΛCDM in any limit here so that $f_5\text{CDM}$ does not represent a deviation from ΛCDM in so much as it is an alternative to it.

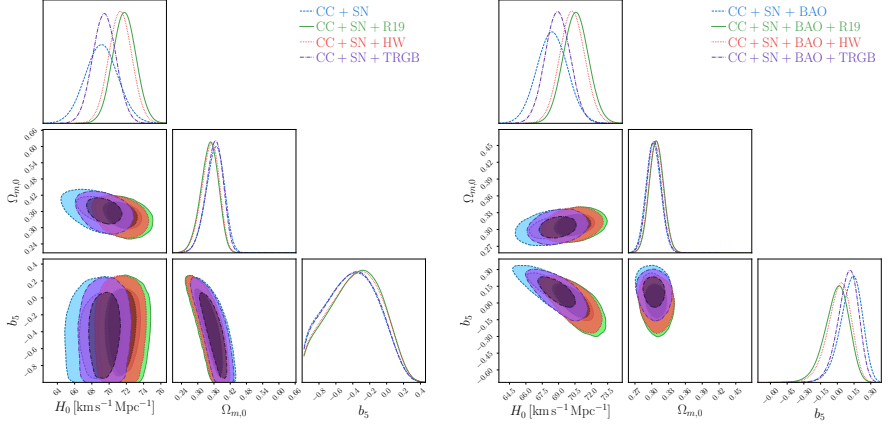


Fig. 5 *Left:* C.L and posteriors for the f_5 CDM model (37) using CC+SN data along the H_0 priors: R19 (green color), HW (red color) and TRGB (purple color), respectively. *Right:* C.L and posteriors for the model (37) using CC+SN+BAO data along the same priors denoted.

Table 5 Results for the hyperbolic tangent model (34). First column: data sets used to constrain the model, including the H_0 priors. Second column: H_0 values derived from the analysis. Third column: Constrained $\Omega_{m,0}$. Fourth column: b_5 best fits. Fifth column: Nuisance parameter, M . Sixth column: χ^2_{\min} . From seventh up to tenth column: AIC and BIC with their respective differences with Λ CDM within the corresponding data set and prior combination (as shown in Appendix A).

Data Sets	H_0 [km/s/Mpc]	$\Omega_{m,0}$	b_5	M	χ^2_{\min}	AIC	BIC	Δ AIC	Δ BIC
CC + SN	$69.2^{+1.9}_{-2.0}$	$0.369^{+0.031}_{-0.036}$	$-0.36^{+0.29}_{-0.38}$	$-19.390^{+0.056}_{-0.058}$	1044.44	1052.44	1072.38	4.95	9.93
CC + SN + R19	71.8 ± 1.3	$0.349^{+0.029}_{-0.035}$	$-0.28^{+0.28}_{-0.38}$	$-19.314^{+0.038}_{-0.041}$	1048.13	1056.13	1076.06	3.81	8.79
CC + SN + HW	71.3 ± 1.3	$0.353^{+0.029}_{-0.036}$	$-0.29^{+0.28}_{-0.38}$	-19.329 ± 0.040	1046.94	1054.94	1074.87	3.94	8.93
CC + SN + TRGB	$69.5^{+1.3}_{-1.4}$	$0.366^{+0.030}_{-0.034}$	$-0.35^{+0.29}_{-0.37}$	$-19.381^{+0.041}_{-0.042}$	1044.50	1052.50	1072.44	4.81	9.80
CC + SN + BAO	$68.4^{+1.5}_{-1.4}$	$0.302^{+0.014}_{-0.012}$	$0.144^{+0.087}_{-0.107}$	$-19.400^{+0.039}_{-0.037}$	1062.88	1070.88	1090.88	7.43	12.43
CC + SN + BAO + R19	$70.6^{+1.1}_{-1.2}$	0.308 ± 0.013	$0.079^{+0.098}_{-0.064}$	$-19.342^{+0.031}_{-0.033}$	1069.77	1077.77	1097.77	3.47	8.47
CC + SN + BAO + HW	70.2 ± 1.1	$0.308^{+0.012}_{-0.013}$	$0.039^{+0.095}_{-0.112}$	$-19.351^{+0.032}_{-0.031}$	1067.90	1075.90	1095.90	3.88	8.88
CC + SN + BAO + TRGB	$68.9^{+1.1}_{-1.2}$	0.304 ± 0.013	$0.115^{+0.082}_{-0.100}$	$-19.386^{+0.032}_{-0.031}$	1063.34	1071.34	1091.34	6.78	11.78

In Fig. 5, the posterior and confidence regions are shown for the f_5 CDM model. As with the f_4 CDM model, our interest in f_5 CDM is in its lack of a Λ CDM limit which removes any preference biases. In contrast to the f_4 CDM model, the model parameter, namely b_5 , does contribute at background level in the f_5 CDM model.

Table 5 shows the precision results for the f_5 CDM model. The situation is now drastically different to that of the f_4 CDM model in that the spread of H_0 values is wider and the density parameter at current times prefers a much larger value. The maximum value of the Hubble constant which is obtained for the CC+SN data set with an R19 prior ($71.8 \pm 1.3 \text{ km s}^{-1} \text{ Mpc}^{-1}$) occurs between the f_2 CDM and f_3 CDM models, while the lowest value is again obtained for the CC+SN+BAO data set with no prior ($68.4^{+1.5}_{-1.4} \text{ km s}^{-1} \text{ Mpc}^{-1}$) on H_0 . Another

issue to point out is that the uncertainties in this scenario are slightly larger than in the cases with a clear Λ CDM limit.

In this scenario the extra model parameter does play a role for the background cosmology and so has an input in the MCMC runs. By and large, the b_5 parameter is within the 2σ region of being zero. However, a significant distinction occurs for the CC+SN and CC+SN+BAO data sets in that the value of b_4 turns out to either be negative or positive respectively. Moreover, the confidence regions are much stricter for the latter case. Another crucial difference between the f_4 CDM and this one is that the statistical indicators are much more realistic in this scenario. Saying that, the Δ AIC and Δ BIC continue to feature a significant distance from Λ CDM. This calls into question whether hyperbolic tangent models are competitive scenarios for cosmology.

While adding more details with the various prior settings under consideration here, we are in agreement with the literature where this model has been investigated [46, 97].

5 Conclusion

Our study probes the impact of H_0 priors in $f(T)$ cosmology using five specific models together with CC, SN and BAO data sets, and 3 particularly relevant cosmology-independent priors from literature. Our interest was in assessing the way in which the cosmological parameters are altered in these various forms of $f(T)$ gravity as well as how they compare statistically with Λ CDM. To make the cross-analysis between the various models, data sets and prior choices more straightforward, we show each of the cosmological parameters against each other in the whisker plot in Fig. ???. Here we also show the value of each prior in shaded regions where the direct impact they have on the cosmological parameters for each model becomes much clearer.

In this work, the first three models we explore in f_1 CDM, f_2 CDM and f_3 CDM are modifications of Λ CDM with a clear-cut limit in this case. We also run our MCMC analysis for Λ CDM which appears in Appendix A which we use for our statistical analysis. These models produce higher values of H_0 and slightly lower values of $\Omega_{m,0}$ as compared with Λ CDM at the expense of an additional model parameter which takes the form of b_i ($i = 1, 2, 3$). This additional freedom in our cosmological model means that we can better approximate the data but produce AIC and BIC values which are higher than in Λ CDM. In our analyses, we find cosmological parameter values that are in agreement with previous works in the literature [46, 49, 97, 98] and within $1-2\sigma$ of Λ CDM.

On the other hand, we also probe the f_4 CDM and f_5 CDM models which are very interesting to explore since they do not have an associated Λ CDM limit, meaning that no set of model parameter values returns an identical Λ CDM behaviour. In fact, in f_4 CDM, the model parameter b_4 does not appear at background level meaning that it has the same number of parameters as Λ CDM in this regime. This also means that we have one less parameter in our MCMC

analyses which means that the number of parameters in the statistical analysis will not be harshly effected by this modified form of gravity. In some case this turns out to be an advantage such as in the CC+SN runs for f_4 CDM which have AIC and BIC values very close to Λ CDM, while for the CC+SN+BAO scenario of Λ CDM give excessively large values for these statistical quantifiers.

The work presented here probes the impact of priors on the Hubble data in the late Universe. It would be interesting to further study this effect using forecast data from future surveys at higher redshift in order to better understand how the cosmological parameters of these models may be effected in comparison to the present analysis. Furthermore, another interesting direction would be to include a perturbative analysis in which growth and gravitational wave data may be included to better probe how these priors effect those associated cosmological parameters. This will be reported elsewhere.

Appendix A Λ CDM Model

In all f_i CDM models we provide comparisons with each respective Λ CDM MCMC run. To this end, we here present the results for Λ CDM for transparency of our results. Firstly in Fig. A1, we show the MCMC posteriors and confidence regions for the various priors for the CC+SN and CC+SN+BAO data sets. As expected, the convergence for each data set and prior combination occurs very fast giving nearly Gaussian uncertainties in every case.

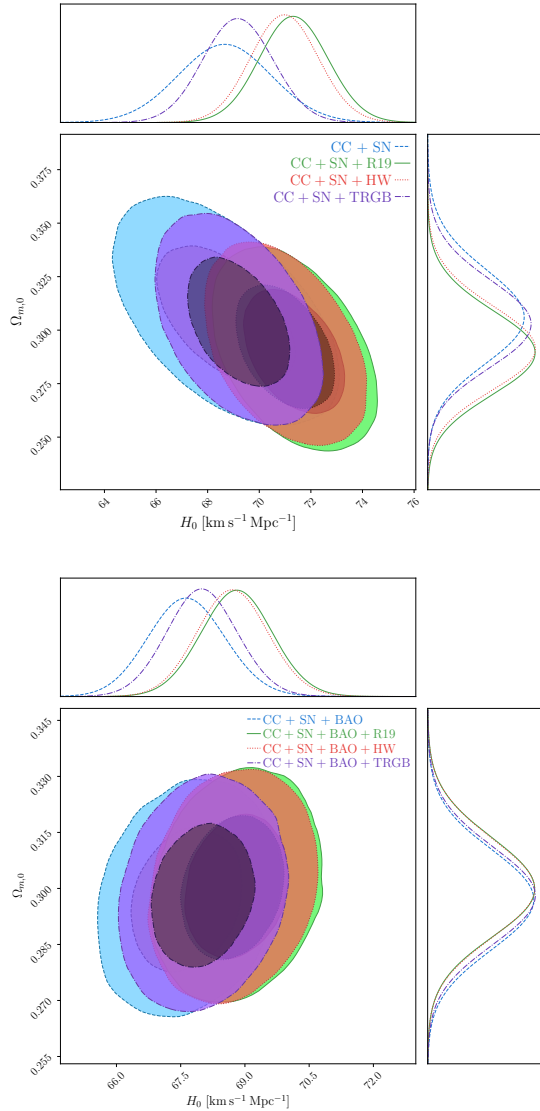


Fig. A1 C.L for the Λ CDM model. *Left:* C.L and posteriors for the model (34) using CC+SN data along the H_0 priors: R19 (green color), HW (red color) and TRGB (purple color), respectively. *Right:* C.L and posteriors for the model (34) using CC+SN+BAO data along the same priors denoted.

Table A1 shows the precision results for each of the MCMC runs with the specific reference values for the AIC and BIC statistical indicators. these are the values used through the work in each of the comparison entries.

Table A1 Results for the Λ CDM model. First column: data sets used to constrain the model, including the H_0 priors. Second column: H_0 values derived from the analysis. Third column: Constrained $\Omega_{m,0}$. Fourth column: χ^2_{\min} . From fifth-sixth column: AIC and BIC results, respectively.

Data Sets	H_0 [kms $^{-1}$ Mpc $^{-1}$]	$\Omega_{m,0}$	χ^2_{\min}	AIC	BIC
CC+ SN	68.7 ± 1.8	$0.306^{+0.022}_{-0.021}$	1041.49	1047.49	1062.44
CC + SN + R19	$71.3^{+1.4}_{-1.3}$	$0.290^{+0.019}_{-0.020}$	1046.32	1052.32	1067.27
CC + SN + HW	71.0 ± 1.3	$0.291^{+0.020}_{-0.019}$	1044.99	1050.99	1065.94
CC + SN + TRGB	69.2 ± 1.4	$0.303^{+0.021}_{-0.020}$	1041.69	1047.69	1062.64
CC + SN + BAO	67.63 ± 0.90	0.297 ± 0.013	1057.46	1063.46	1078.45
CC + SN + BAO + R19	$68.81^{+0.82}_{-0.84}$	0.300 ± 0.013	1068.30	1074.30	1089.30
CC + SN + BAO + HW	68.70 ± 0.83	$0.300^{+0.014}_{-0.013}$	1066.03	1072.03	1087.03
CC + SN + BAO + TRGB	$67.98^{+0.85}_{-0.81}$	0.298 ± 0.013	1058.56	1064.56	1079.56

Acknowledgments The authors would like to acknowledge networking support by the COST Action CA18108 and funding support from Cosmology@MALTA which is supported by the University of Malta. This research has been carried out using computational facilities procured through the European Regional Development Fund, Project No. ERDF-080 “A supercomputing laboratory for the University of Malta”. The authors would also like to acknowledge funding from “The Malta Council for Science and Technology” in project IPAS-2020-007. CE-R acknowledges the Royal Astronomical Society as FRAS 10147 and by DGAPA-PAPIIT-UNAM Project IA100220.

References

- [1] Bernal, J.L., Verde, L., Riess, A.G.: The trouble with H_0 . *JCAP* **10**, 019 (2016) [arXiv:1607.05617](https://arxiv.org/abs/1607.05617) [astro-ph.CO]. <https://doi.org/10.1088/1475-7516/2016/10/019>
- [2] Di Valentino, E., *et al.*: Snowmass2021 - Letter of interest cosmology intertwined II: The hubble constant tension. *Astropart. Phys.* **131**, 102605 (2021) [arXiv:2008.11284](https://arxiv.org/abs/2008.11284) [astro-ph.CO]. <https://doi.org/10.1016/j.astropartphys.2021.102605>
- [3] Di Valentino, E., Mena, O., Pan, S., Visinelli, L., Yang, W., Melchiorri, A., Mota, D.F., Riess, A.G., Silk, J.: In the Realm of the Hubble tension – a Review of Solutions (2021) [arXiv:2103.01183](https://arxiv.org/abs/2103.01183) [astro-ph.CO]. <https://doi.org/10.1088/1361-6382/ac086d>
- [4] Aghanim, N., *et al.*: Planck 2018 results. VI. Cosmological parameters. *Astron. Astrophys.* **641**, 6 (2020) [arXiv:1807.06209](https://arxiv.org/abs/1807.06209) [astro-ph.CO]. <https://doi.org/10.1051/0004-6361/201833910>
- [5] Baudis, L.: Dark matter detection. *J. Phys. G* **43**(4), 044001 (2016).

<https://doi.org/10.1088/0954-3899/43/4/044001>

- [6] Bertone, G., Hooper, D., Silk, J.: Particle dark matter: Evidence, candidates and constraints. *Phys. Rept.* **405**, 279–390 (2005) [arXiv:hep-ph/0404175](https://arxiv.org/abs/hep-ph/0404175). <https://doi.org/10.1016/j.physrep.2004.08.031>
- [7] Peebles, P.J.E., Ratra, B.: The Cosmological Constant and Dark Energy. *Rev. Mod. Phys.* **75**, 559–606 (2003) [arXiv:astro-ph/0207347](https://arxiv.org/abs/astro-ph/0207347). <https://doi.org/10.1103/RevModPhys.75.559>
- [8] Copeland, E.J., Sami, M., Tsujikawa, S.: Dynamics of dark energy. *Int. J. Mod. Phys. D* **15**, 1753–1936 (2006) [arXiv:hep-th/0603057](https://arxiv.org/abs/hep-th/0603057). <https://doi.org/10.1142/S021827180600942X>
- [9] Riess, A.G., *et al.*: Observational evidence from supernovae for an accelerating universe and a cosmological constant. *Astron. J.* **116**, 1009–1038 (1998) [arXiv:astro-ph/9805201](https://arxiv.org/abs/astro-ph/9805201). <https://doi.org/10.1086/300499>
- [10] Perlmutter, S., *et al.*: Measurements of Ω and Λ from 42 high redshift supernovae. *Astrophys. J.* **517**, 565–586 (1999) [arXiv:astro-ph/9812133](https://arxiv.org/abs/astro-ph/9812133). <https://doi.org/10.1086/307221>
- [11] Gaitskell, R.J.: Direct detection of dark matter. *Ann. Rev. Nucl. Part. Sci.* **54**, 315–359 (2004). <https://doi.org/10.1146/annurev.nucl.54.070103.181244>
- [12] Weinberg, S.: The Cosmological Constant Problem. *Rev. Mod. Phys.* **61**, 1–23 (1989). <https://doi.org/10.1103/RevModPhys.61.1>
- [13] Riess, A.G., Casertano, S., Yuan, W., Macri, L.M., Scolnic, D.: Large Magellanic Cloud Cepheid Standards Provide a 1% Foundation for the Determination of the Hubble Constant and Stronger Evidence for Physics beyond Λ CDM. *Astrophys. J.* **876**(1), 85 (2019) [arXiv:1903.07603](https://arxiv.org/abs/1903.07603) [astro-ph.CO]. <https://doi.org/10.3847/1538-4357/ab1422>
- [14] Wong, K.C., *et al.*: H0LiCOW XIII. A 2.4% measurement of H_0 from lensed quasars: 5.3 σ tension between early and late-Universe probes (2019) [arXiv:1907.04869](https://arxiv.org/abs/1907.04869) [astro-ph.CO]
- [15] Abbott, T.M.C., *et al.*: Dark Energy Survey Year 3 Results: Cosmological Constraints from Galaxy Clustering and Weak Lensing (2021) [arXiv:2105.13549](https://arxiv.org/abs/2105.13549) [astro-ph.CO]
- [16] Graef, L.L., Benetti, M., Alcaniz, J.S.: Primordial gravitational waves and the H_0 -tension problem. *Phys. Rev. D* **99**(4), 043519 (2019) [arXiv:1809.04501](https://arxiv.org/abs/1809.04501) [astro-ph.CO]. <https://doi.org/10.1103/PhysRevD.99.043519>

043519

- [17] Abbott, B.P., *et al.*: A gravitational-wave standard siren measurement of the Hubble constant. *Nature* **551**(7678), 85–88 (2017) [arXiv:1710.05835](#) [astro-ph.CO]. <https://doi.org/10.1038/nature24471>
- [18] Baker, J., *et al.*: The Laser Interferometer Space Antenna: Unveiling the Millihertz Gravitational Wave Sky (2019) [arXiv:1907.06482](#) [astro-ph.IM]
- [19] Amaro-Seoane, P., Audley, H., *et al.*: Laser Interferometer Space Antenna. *arXiv e-prints*, 1702–00786 (2017) [arXiv:1702.00786](#) [astro-ph.IM]
- [20] Sotiriou, T.P., Faraoni, V.: $f(R)$ Theories Of Gravity. *Rev. Mod. Phys.* **82**, 451–497 (2010) [arXiv:0805.1726](#) [gr-qc]. <https://doi.org/10.1103/RevModPhys.82.451>
- [21] Clifton, T., Ferreira, P.G., Padilla, A., Skordis, C.: Modified Gravity and Cosmology. *Phys. Rept.* **513**, 1–189 (2012) [arXiv:1106.2476](#) [astro-ph.CO]. <https://doi.org/10.1016/j.physrep.2012.01.001>
- [22] Saridakis, E.N., *et al.*: Modified Gravity and Cosmology: An Update by the CANTATA Network (2021) [arXiv:2105.12582](#) [gr-qc]
- [23] Faraoni, V.: $f(R)$ gravity: Successes and challenges. In: 18th SIGRAV Conference (2008)
- [24] Capozziello, S., De Laurentis, M.: Extended Theories of Gravity. *Phys. Rept.* **509**, 167–321 (2011) [arXiv:1108.6266](#) [gr-qc]. <https://doi.org/10.1016/j.physrep.2011.09.003>
- [25] Misner, C.W., Thorne, K.S., Wheeler, J.A.: *Gravitation*. Gravitation, vol. pt. 3. W. H. Freeman, ??? (1973). <https://books.google.com.mt/books?id=w4Gigq3tY1kC>
- [26] Nakahara, M.: *Geometry, Topology and Physics*, Second Edition. Graduate student series in physics. Taylor & Francis, ??? (2003). <https://books.google.com.mt/books?id=cH-XQB0Ex5wC>
- [27] Bahamonde, S., Dialektopoulos, K.F., Escamilla-Rivera, C., Farrugia, G., Gakis, V., Hendry, M., Hohmann, M., Said, J.L., Mifsud, J., Di Valentino, E.: Teleparallel Gravity: From Theory to Cosmology (2021) [arXiv:2106.13793](#) [gr-qc]
- [28] Aldrovandi, R., Pereira, J.G.: *Teleparallel Gravity: An Introduction*. Springer, ??? (2013). <https://doi.org/10.1007/978-94-007-5143-9>

- [29] Cai, Y.-F., Capozziello, S., De Laurentis, M., Saridakis, E.N.: $f(T)$ teleparallel gravity and cosmology. Rept. Prog. Phys. **79**(10), 106901 (2016) [arXiv:1511.07586](https://arxiv.org/abs/1511.07586) [gr-qc]. <https://doi.org/10.1088/0034-4885/79/10/106901>
- [30] Krssak, M., van den Hoogen, R.J., Pereira, J.G., Böhmer, C.G., Coley, A.A.: Teleparallel theories of gravity: illuminating a fully invariant approach. Class. Quant. Grav. **36**(18), 183001 (2019) [arXiv:1810.12932](https://arxiv.org/abs/1810.12932) [gr-qc]. <https://doi.org/10.1088/1361-6382/ab2e1f>
- [31] Weitzenböck, R.: ‘Invariantentheorie’. Noordhoff, Gronningen, ??? (1923)
- [32] Lovelock, D.: The Einstein tensor and its generalizations. J. Math. Phys. **12**, 498–501 (1971). <https://doi.org/10.1063/1.1665613>
- [33] Gonzalez, P.A., Vasquez, Y.: Teleparallel Equivalent of Lovelock Gravity. Phys. Rev. D **92**(12), 124023 (2015) [arXiv:1508.01174](https://arxiv.org/abs/1508.01174) [hep-th]. <https://doi.org/10.1103/PhysRevD.92.124023>
- [34] Bahamonde, S., Dialektopoulos, K.F., Levi Said, J.: Can Horndeski Theory be recast using Teleparallel Gravity? Phys. Rev. D **100**(6), 064018 (2019) [arXiv:1904.10791](https://arxiv.org/abs/1904.10791) [gr-qc]. <https://doi.org/10.1103/PhysRevD.100.064018>
- [35] Ferraro, R., Fiorini, F.: Modified teleparallel gravity: Inflation without inflaton. Phys. Rev. **D75**, 084031 (2007) [arXiv:gr-qc/0610067](https://arxiv.org/abs/gr-qc/0610067) [gr-qc]. <https://doi.org/10.1103/PhysRevD.75.084031>
- [36] Ferraro, R., Fiorini, F.: On Born-Infeld Gravity in Weitzenböck spacetime. Phys. Rev. **D78**, 124019 (2008) [arXiv:0812.1981](https://arxiv.org/abs/0812.1981) [gr-qc]. <https://doi.org/10.1103/PhysRevD.78.124019>
- [37] Bengochea, G.R., Ferraro, R.: Dark torsion as the cosmic speed-up. Phys. Rev. **D79**, 124019 (2009) [arXiv:0812.1205](https://arxiv.org/abs/0812.1205) [astro-ph]. <https://doi.org/10.1103/PhysRevD.79.124019>
- [38] Linder, E.V.: Einstein’s Other Gravity and the Acceleration of the Universe. Phys. Rev. **D81**, 127301 (2010) [arXiv:1005.3039](https://arxiv.org/abs/1005.3039) [astro-ph.CO]. <https://doi.org/10.1103/PhysRevD.81.127301>, <https://doi.org/10.1103/PhysRevD.82.109902>. [Erratum: Phys. Rev.D82,109902(2010)]
- [39] Chen, S.-H., Dent, J.B., Dutta, S., Saridakis, E.N.: Cosmological perturbations in $f(T)$ gravity. Phys. Rev. **D83**, 023508 (2011) [arXiv:1008.1250](https://arxiv.org/abs/1008.1250) [astro-ph.CO]. <https://doi.org/10.1103/PhysRevD.83.023508>

- [40] Bahamonde, S., Flathmann, K., Pfeifer, C.: Photon sphere and perihelion shift in weak $f(T)$ gravity. *Phys. Rev. D* **100**(8), 084064 (2019) [arXiv:1907.10858](https://arxiv.org/abs/1907.10858) [gr-qc]. <https://doi.org/10.1103/PhysRevD.100.084064>
- [41] Farrugia, G., Levi Said, J.: Stability of the flat FLRW metric in $f(T)$ gravity. *Phys. Rev. D* **94**(12), 124054 (2016) [arXiv:1701.00134](https://arxiv.org/abs/1701.00134) [gr-qc]. <https://doi.org/10.1103/PhysRevD.94.124054>
- [42] Finch, A., Said, J.L.: Galactic Rotation Dynamics in $f(T)$ gravity. *Eur. Phys. J. C* **78**(7), 560 (2018) [arXiv:1806.09677](https://arxiv.org/abs/1806.09677) [astro-ph.GA]. <https://doi.org/10.1140/epjc/s10052-018-6028-1>
- [43] Farrugia, G., Levi Said, J., Ruggiero, M.L.: Solar System tests in $f(T)$ gravity. *Phys. Rev. D* **93**(10), 104034 (2016) [arXiv:1605.07614](https://arxiv.org/abs/1605.07614) [gr-qc]. <https://doi.org/10.1103/PhysRevD.93.104034>
- [44] Iorio, L., Saridakis, E.N.: Solar system constraints on $f(T)$ gravity. *Mon. Not. Roy. Astron. Soc.* **427**, 1555 (2012) [arXiv:1203.5781](https://arxiv.org/abs/1203.5781) [gr-qc]. <https://doi.org/10.1111/j.1365-2966.2012.21995.x>
- [45] Deng, X.-M.: Probing $f(T)$ gravity with gravitational time advancement. *Class. Quant. Grav.* **35**(17), 175013 (2018). <https://doi.org/10.1088/1361-6382/aad391>
- [46] Nesseris, S., Basilakos, S., Saridakis, E.N., Perivolaropoulos, L.: Viable $f(T)$ models are practically indistinguishable from Λ CDM. *Phys. Rev. D* **88**, 103010 (2013) [arXiv:1308.6142](https://arxiv.org/abs/1308.6142) [astro-ph.CO]. <https://doi.org/10.1103/PhysRevD.88.103010>
- [47] Anagnostopoulos, F.K., Basilakos, S., Saridakis, E.N.: Bayesian analysis of $f(T)$ gravity using $f\sigma_8$ data. *Phys. Rev. D* **100**(8), 083517 (2019) [arXiv:1907.07533](https://arxiv.org/abs/1907.07533) [astro-ph.CO]. <https://doi.org/10.1103/PhysRevD.100.083517>
- [48] Nunes, R.C., Pan, S., Saridakis, E.N.: New observational constraints on $f(T)$ gravity through gravitational-wave astronomy. *Phys. Rev. D* **98**(10), 104055 (2018) [arXiv:1810.03942](https://arxiv.org/abs/1810.03942) [gr-qc]. <https://doi.org/10.1103/PhysRevD.98.104055>
- [49] Benetti, M., Capozziello, S., Lambiase, G.: Updating constraints on $f(T)$ teleparallel cosmology and the consistency with Big Bang Nucleosynthesis. *Mon. Not. Roy. Astron. Soc.* **500**(2), 1795–1805 (2020) [arXiv:2006.15335](https://arxiv.org/abs/2006.15335) [astro-ph.CO]. <https://doi.org/10.1093/mnras/staa3368>
- [50] Bahamonde, S., Böhmer, C.G., Wright, M.: Modified teleparallel theories

- of gravity. Phys. Rev. D **92**(10), 104042 (2015) [arXiv:1508.05120](https://arxiv.org/abs/1508.05120) [gr-qc]. <https://doi.org/10.1103/PhysRevD.92.104042>
- [51] Bahamonde, S., Capozziello, S.: Noether Symmetry Approach in $f(T, B)$ teleparallel cosmology. Eur. Phys. J. C **77**(2), 107 (2017) [arXiv:1612.01299](https://arxiv.org/abs/1612.01299) [gr-qc]. <https://doi.org/10.1140/epjc/s10052-017-4677-0>
- [52] Paliathanasis, A.: de Sitter and Scaling solutions in a higher-order modified teleparallel theory. JCAP **08**, 027 (2017) [arXiv:1706.02662](https://arxiv.org/abs/1706.02662) [gr-qc]. <https://doi.org/10.1088/1475-7516/2017/08/027>
- [53] Farrugia, G., Levi Said, J., Gakis, V., Saridakis, E.N.: Gravitational Waves in Modified Teleparallel Theories. Phys. Rev. D **97**(12), 124064 (2018) [arXiv:1804.07365](https://arxiv.org/abs/1804.07365) [gr-qc]. <https://doi.org/10.1103/PhysRevD.97.124064>
- [54] Bahamonde, S., Zubair, M., Abbas, G.: Thermodynamics and cosmological reconstruction in $f(T, B)$ gravity. Phys. Dark Univ. **19**, 78–90 (2018) [arXiv:1609.08373](https://arxiv.org/abs/1609.08373) [gr-qc]. <https://doi.org/10.1016/j.dark.2017.12.005>
- [55] Wright, M.: Conformal transformations in modified teleparallel theories of gravity revisited. Phys. Rev. D **93**(10), 103002 (2016) [arXiv:1602.05764](https://arxiv.org/abs/1602.05764) [gr-qc]. <https://doi.org/10.1103/PhysRevD.93.103002>
- [56] Farrugia, G., Levi Said, J., Finch, A.: Gravitoelectromagnetism, Solar System Tests, and Weak-Field Solutions in $f(T, B)$ Gravity with Observational Constraints. Universe **6**(2), 34 (2020) [arXiv:2002.08183](https://arxiv.org/abs/2002.08183) [gr-qc]. <https://doi.org/10.3390/universe6020034>
- [57] Capozziello, S., Capriolo, M., Caso, L.: Weak field limit and gravitational waves in $f(T, B)$ teleparallel gravity. Eur. Phys. J. C **80**(2), 156 (2020) [arXiv:1912.12469](https://arxiv.org/abs/1912.12469) [gr-qc]. <https://doi.org/10.1140/epjc/s10052-020-7737-9>
- [58] Escamilla-Rivera, C., Levi Said, J.: Cosmological viable models in $f(T, B)$ theory as solutions to the H_0 tension. Class. Quant. Grav. **37**(16), 165002 (2020) [arXiv:1909.10328](https://arxiv.org/abs/1909.10328) [gr-qc]. <https://doi.org/10.1088/1361-6382/ab939c>
- [59] Kofinas, G., Saridakis, E.N.: Teleparallel equivalent of Gauss-Bonnet gravity and its modifications. Phys. Rev. D **90**, 084044 (2014) [arXiv:1404.2249](https://arxiv.org/abs/1404.2249) [gr-qc]. <https://doi.org/10.1103/PhysRevD.90.084044>
- [60] Kofinas, G., Saridakis, E.N.: Cosmological applications of $F(T, T_G)$ gravity. Phys. Rev. D **90**, 084045 (2014) [arXiv:1408.0107](https://arxiv.org/abs/1408.0107) [gr-qc]. <https://doi.org/10.1103/PhysRevD.90.084045>

- [61] de la Cruz-Dombriz, A., Farrugia, G., Said, J.L., Saez-Gomez, D.: Cosmological reconstructed solutions in extended teleparallel gravity theories with a teleparallel Gauss–Bonnet term. *Class. Quant. Grav.* **34**(23), 235011 (2017) [arXiv:1705.03867](https://arxiv.org/abs/1705.03867) [gr-qc]. <https://doi.org/10.1088/1361-6382/aa93c8>
- [62] de la Cruz-Dombriz, A., Farrugia, G., Said, J.L., Sáez-Chillón Gómez, D.: Cosmological bouncing solutions in extended teleparallel gravity theories. *Phys. Rev. D* **97**(10), 104040 (2018) [arXiv:1801.10085](https://arxiv.org/abs/1801.10085) [gr-qc]. <https://doi.org/10.1103/PhysRevD.97.104040>
- [63] Bahamonde, S., Dialektopoulos, K.F., Gakis, V., Levi Said, J.: Reviving Horndeski theory using teleparallel gravity after GW170817. *Phys. Rev. D* **101**(8), 084060 (2020) [arXiv:1907.10057](https://arxiv.org/abs/1907.10057) [gr-qc]. <https://doi.org/10.1103/PhysRevD.101.084060>
- [64] Bahamonde, S., Dialektopoulos, K.F., Hohmann, M., Levi Said, J.: Post-Newtonian limit of Teleparallel Horndeski gravity. *Class. Quant. Grav.* **38**(2), 025006 (2020) [arXiv:2003.11554](https://arxiv.org/abs/2003.11554) [gr-qc]. <https://doi.org/10.1088/1361-6382/abc441>
- [65] Hohmann, M., Järv, L., Krššák, M., Pfeifer, C.: Modified teleparallel theories of gravity in symmetric spacetimes. *Phys. Rev. D* **100**(8), 084002 (2019) [arXiv:1901.05472](https://arxiv.org/abs/1901.05472) [gr-qc]. <https://doi.org/10.1103/PhysRevD.100.084002>
- [66] Hayashi, K., Shirafuji, T.: New General Relativity. *Phys. Rev. D* **19**, 3524–3553 (1979). <https://doi.org/10.1103/PhysRevD.19.3524>. [Addendum: *Phys.Rev.D* 24, 3312–3314 (1982)]
- [67] Chandrasekhar, S.: The Mathematical Theory of Black Holes. *Fundam. Theor. Phys.* **9**, 5–26 (1984). https://doi.org/10.1007/978-94-009-6469-3_2
- [68] De Felice, A., Tsujikawa, S.: $f(R)$ theories. *Living Rev. Rel.* **13**, 3 (2010) [arXiv:1002.4928](https://arxiv.org/abs/1002.4928) [gr-qc]. <https://doi.org/10.12942/lrr-2010-3>
- [69] Rezaei Akbarieh, A., Izadi, Y.: Tachyon Inflation in Teleparallel Gravity. *Eur. Phys. J. C* **79**(4), 366 (2019) [arXiv:1812.06649](https://arxiv.org/abs/1812.06649) [gr-qc]. <https://doi.org/10.1140/epjc/s10052-019-6819-z>
- [70] Krššák, M., Saridakis, E.N.: The covariant formulation of $f(T)$ gravity. *Class. Quant. Grav.* **33**(11), 115009 (2016) [arXiv:1510.08432](https://arxiv.org/abs/1510.08432) [gr-qc]. <https://doi.org/10.1088/0264-9381/33/11/115009>
- [71] Tamanini, N., Boehmer, C.G.: Good and bad tetrads in $f(T)$ gravity. *Phys. Rev. D* **86**, 044009 (2012) [arXiv:1204.4593](https://arxiv.org/abs/1204.4593) [gr-qc]. <https://doi.org/10.1103/PhysRevD.86.044009>

[org/10.1103/PhysRevD.86.044009](https://doi.org/10.1103/PhysRevD.86.044009)

- [72] Jimenez, R., Loeb, A.: Constraining cosmological parameters based on relative galaxy ages. *Astrophys. J.* **573**, 37–42 (2002) [arXiv:astro-ph/0106145](https://arxiv.org/abs/astro-ph/0106145) [astro-ph]. <https://doi.org/10.1086/340549>
- [73] Zhang, C., Zhang, H., Yuan, S., Liu, S., Zhang, T.-J., Sun, Y.-C.: Four new observational $H(z)$ data from luminous red galaxies in the Sloan Digital Sky Survey data release seven. *Research in Astronomy and Astrophysics* **14**(10), 1221–1233 (2014) [arXiv:1207.4541](https://arxiv.org/abs/1207.4541) [astro-ph.CO]. <https://doi.org/10.1088/1674-4527/14/10/002>
- [74] Jimenez, R., Verde, L., Treu, T., Stern, D.: Constraints on the equation of state of dark energy and the Hubble constant from stellar ages and the CMB. *Astrophys. J.* **593**, 622–629 (2003) [arXiv:astro-ph/0302560](https://arxiv.org/abs/astro-ph/0302560). <https://doi.org/10.1086/376595>
- [75] Moresco, M., Pozzetti, L., Cimatti, A., Jimenez, R., Maraston, C., Verde, L., Thomas, D., Citro, A., Tojeiro, R., Wilkinson, D.: A 6% measurement of the Hubble parameter at $z \sim 0.45$: direct evidence of the epoch of cosmic re-acceleration. *JCAP* **05**, 014 (2016) [arXiv:1601.01701](https://arxiv.org/abs/1601.01701) [astro-ph.CO]. <https://doi.org/10.1088/1475-7516/2016/05/014>
- [76] Simon, J., Verde, L., Jimenez, R.: Constraints on the redshift dependence of the dark energy potential. *Phys. Rev. D* **71**, 123001 (2005) [arXiv:astro-ph/0412269](https://arxiv.org/abs/astro-ph/0412269). <https://doi.org/10.1103/PhysRevD.71.123001>
- [77] Moresco, M., Cimatti, A., Jimenez, R., Pozzetti, L., Zamorani, G., Bolzonella, M., Dunlop, J., Lamareille, F., Mignoli, M., Pearce, H., Rosati, P., Stern, D., Verde, L., Zucca, E., Carollo, C.M., Contini, T., Kneib, J.-P., Le Fèvre, O., Lilly, S.J., Mainieri, V., Renzini, A., Scodreggio, M., Balestra, I., Gobat, R., McLure, R., Bardelli, S., Bongiorno, A., Caputi, K., Cucciati, O., de la Torre, S., de Ravel, L., Franzetti, P., Garilli, B., Iovino, A., Kampczyk, P., Knobel, C., Kovač, K., Le Borgne, J.-F., Le Brun, V., Maier, C., Pelló, R., Peng, Y., Perez-Montero, E., Presotto, V., Silverman, J.D., Tanaka, M., Tasca, L.A.M., Tresse, L., Vergani, D., Almaini, O., Barnes, L., Bordoloi, R., Bradshaw, E., Cappi, A., Chuter, R., Cirasuolo, M., Coppa, G., Diener, C., Foucaud, S., Hartley, W., Kamionkowski, M., Koekemoer, A.M., López-Sanjuan, C., McCracken, H.J., Nair, P., Oesch, P., Stanford, A., Welikala, N.: Improved constraints on the expansion rate of the Universe up to $z \sim 1.1$ from the spectroscopic evolution of cosmic chronometers. *JCAP* **2012**(8), 006 (2012) [arXiv:1201.3609](https://arxiv.org/abs/1201.3609) [astro-ph.CO]. <https://doi.org/10.1088/1475-7516/2012/08/006>
- [78] Stern, D., Jimenez, R., Verde, L., Kamionkowski, M., Stanford, S.A.: Cosmic chronometers: constraining the equation of state of dark energy.

- I: $H(z)$ measurements. JCAP **2010**(2), 008 (2010) [arXiv:0907.3149](https://arxiv.org/abs/0907.3149) [astro-ph.CO]. <https://doi.org/10.1088/1475-7516/2010/02/008>
- [79] Moresco, M.: Raising the bar: new constraints on the Hubble parameter with cosmic chronometers at $z \sim 2$. Mon. Not. Roy. Astron. Soc. **450**(1), 16–20 (2015) [arXiv:1503.01116](https://arxiv.org/abs/1503.01116) [astro-ph.CO]. <https://doi.org/10.1093/mnrasl/slv037>
- [80] Gómez-Valent, A., Amendola, L.: H_0 from cosmic chronometers and Type Ia supernovae, with Gaussian Processes and the novel Weighted Polynomial Regression method. JCAP **04**, 051 (2018) [arXiv:1802.01505](https://arxiv.org/abs/1802.01505) [astro-ph.CO]. <https://doi.org/10.1088/1475-7516/2018/04/051>
- [81] Lopez-Corredoira, M., Vazdekis, A., Gutierrez, C.M., Castro-Rodriguez, N.: Stellar content of extremely red quiescent galaxies at $z > 2$. Astron. Astrophys. **600**, 91 (2017) [arXiv:1702.00380](https://arxiv.org/abs/1702.00380) [astro-ph.GA]. <https://doi.org/10.1051/0004-6361/201629857>
- [82] Lopez-Corredoira, M., Vazdekis, A.: Impact of young stellar components on quiescent galaxies: deconstructing cosmic chronometers. Astron. Astrophys. **614**, 127 (2018) [arXiv:1802.09473](https://arxiv.org/abs/1802.09473) [astro-ph.CO]. <https://doi.org/10.1051/0004-6361/201731647>
- [83] Verde, L., Protopapas, P., Jimenez, R.: The expansion rate of the intermediate Universe in light of Planck. Phys. Dark Univ. **5-6**, 307–314 (2014) [arXiv:1403.2181](https://arxiv.org/abs/1403.2181) [astro-ph.CO]. <https://doi.org/10.1016/j.dark.2014.09.003>
- [84] Scolnic, D.M., *et al.*: The complete light-curve sample of spectroscopically confirmed SNe Ia from Pan-STARRS1 and cosmological constraints from the combined Pantheon Sample. Astrophys. J. **859**(2), 101 (2018) [arXiv:1710.00845](https://arxiv.org/abs/1710.00845) [astro-ph.CO]. <https://doi.org/10.3847/1538-4357/aab9bb>
- [85] Conley, A., Guy, J., Sullivan, M., Regnault, N., Astier, P., Balland, C., Basa, S., Carlberg, R.G., Fouchez, D., Hardin, D., Hook, I.M., Howell, D.A., Pain, R., Palanque-Delabrouille, N., Perrett, K.M., Pritchett, C.J., Rich, J., Ruhlmann-Kleider, V., Balam, D., Baumont, S., Ellis, R.S., Fabbro, S., Fakhouri, H.K., Fourmanoit, N., González-Gaitán, S., Graham, M.L., Hudson, M.J., Hsiao, E., Kronborg, T., Lidman, C., Mourao, A.M., Neill, J.D., Perlmutter, S., Ripoche, P., Suzuki, N., Walker, E.S.: Supernova Constraints and Systematic Uncertainties from the First Three Years of the Supernova Legacy Survey. The Astrophysical Journal **192**(1), 1 (2011) [arXiv:1104.1443](https://arxiv.org/abs/1104.1443) [astro-ph.CO]. <https://doi.org/10.1088/0067-0049/192/1/1>

- [86] Ross, A.J., Samushia, L., Howlett, C., Percival, W.J., Burden, A., Manera, M.: The clustering of the SDSS DR7 main Galaxy sample – I. A 4 per cent distance measure at $z = 0.15$. *Mon. Not. Roy. Astron. Soc.* **449**(1), 835–847 (2015) [arXiv:1409.3242](#) [astro-ph.CO]. <https://doi.org/10.1093/mnras/stv154>
- [87] Beutler, F., Blake, C., Colless, M., Jones, D.H., Staveley-Smith, L., Campbell, L., Parker, Q., Saunders, W., Watson, F.: The 6dF Galaxy Survey: baryon acoustic oscillations and the local Hubble constant. *Monthly Notices of the Royal Astronomical Society* **416**(4), 3017–3032 (2011) [arXiv:1106.3366](#) [astro-ph.CO]. <https://doi.org/10.1111/j.1365-2966.2011.19250.x>
- [88] du Mas des Bourboux, H., *et al.*: Baryon acoustic oscillations from the complete SDSS-III Ly α -quasar cross-correlation function at $z = 2.4$. *Astron. Astrophys.* **608**, 130 (2017) [arXiv:1708.02225](#) [astro-ph.CO]. <https://doi.org/10.1051/0004-6361/201731731>
- [89] Zhao, G.-B., *et al.*: The clustering of the SDSS-IV extended Baryon Oscillation Spectroscopic Survey DR14 quasar sample: a tomographic measurement of cosmic structure growth and expansion rate based on optimal redshift weights. *Mon. Not. Roy. Astron. Soc.* **482**(3), 3497–3513 (2019) [arXiv:1801.03043](#) [astro-ph.CO]. <https://doi.org/10.1093/mnras/sty2845>
- [90] Alam, S., *et al.*: The clustering of galaxies in the completed SDSS-III Baryon Oscillation Spectroscopic Survey: cosmological analysis of the DR12 galaxy sample. *Mon. Not. Roy. Astron. Soc.* **470**(3), 2617–2652 (2017) [arXiv:1607.03155](#) [astro-ph.CO]. <https://doi.org/10.1093/mnras/stx721>
- [91] Fixsen, D.J.: The Temperature of the Cosmic Microwave Background. *The Astrophysical Journal* **707**(2), 916–920 (2009) [arXiv:0911.1955](#) [astro-ph.CO]. <https://doi.org/10.1088/0004-637X/707/2/916>
- [92] Freedman, W.L., *et al.*: The Carnegie-Chicago Hubble Program. VIII. An independent determination of the Hubble constant based on the Tip of the Red Giant Branch. *Astrophys. J.* **882**(1), 34 (2019) [arXiv:1907.05922](#) [astro-ph.CO]. <https://doi.org/10.3847/1538-4357/ab2f73>
- [93] Akaike, H.: A new look at the statistical model identification. *IEEE Transactions on Automatic Control* **19**(6), 716–723 (1974). <https://doi.org/10.1109/TAC.1974.1100705>
- [94] Schwarz, G.: Estimating the Dimension of a Model. *The Annals of Statistics* **6**(2), 461–464 (1978). <https://doi.org/10.1214/aos/1176344136>

- [95] Dvali, G.R., Gabadadze, G., Porrati, M.: 4-D gravity on a brane in 5-D Minkowski space. *Phys. Lett. B* **485**, 208–214 (2000) [arXiv:hep-th/0005016](https://arxiv.org/abs/hep-th/0005016). [https://doi.org/10.1016/S0370-2693\(00\)00669-9](https://doi.org/10.1016/S0370-2693(00)00669-9)
- [96] Bárcenas-Enríquez, G., Escamilla-Rivera, C., Garcia-Aspeitia, M.A.: Cosmological analysis of a Dvali-Gabadadze-Porrati stable model with $H(z)$ observations. *Rev. Mex. Fis.* **64**(6), 584–589 (2018) [arXiv:1803.03283](https://arxiv.org/abs/1803.03283) [gr-qc]. <https://doi.org/10.31349/RevMexFis.64.584>
- [97] Xu, B., Yu, H., Wu, P.: Testing Viable $f(T)$ Models with Current Observations. *The Astrophysical Journal* **855**(2), 89 (2018). <https://doi.org/10.3847/1538-4357/aaad12>
- [98] Wang, D., Mota, D.: Can $f(T)$ gravity resolve the H_0 tension? *Phys. Rev. D* **102**(6), 063530 (2020) [arXiv:2003.10095](https://arxiv.org/abs/2003.10095) [astro-ph.CO]. <https://doi.org/10.1103/PhysRevD.102.063530>
- [99] Linder, E.V.: Exponential Gravity. *Phys. Rev. D* **80**, 123528 (2009) [arXiv:0905.2962](https://arxiv.org/abs/0905.2962) [astro-ph.CO]. <https://doi.org/10.1103/PhysRevD.80.123528>
- [100] Bamba, K., Geng, C.-Q., Lee, C.-C., Luo, L.-W.: Equation of state for dark energy in $f(T)$ gravity. *JCAP* **01**, 021 (2011) [arXiv:1011.0508](https://arxiv.org/abs/1011.0508) [astro-ph.CO]. <https://doi.org/10.1088/1475-7516/2011/01/021>
- [101] Deffayet, C.: Cosmology on a brane in Minkowski bulk. *Phys. Lett. B* **502**, 199–208 (2001) [arXiv:hep-th/0010186](https://arxiv.org/abs/hep-th/0010186). [https://doi.org/10.1016/S0370-2693\(01\)00160-5](https://doi.org/10.1016/S0370-2693(01)00160-5)
- [102] Wu, P., Yu, H.W.: $f(T)$ models with phantom divide line crossing. *Eur. Phys. J. C* **71**, 1552 (2011) [arXiv:1008.3669](https://arxiv.org/abs/1008.3669) [gr-qc]. <https://doi.org/10.1140/epjc/s10052-011-1552-2>